Forward Planar Projection Through Layered Media

Gregory T. Clement and Kullervo Hynynen, *Member, IEEE*

***Abstract*—A planar forward projection algorithm is combined with ray theory to describe longitudinal propagation through an arbitrary number of randomly oriented isotropic layers. This method first measures the space-time pressure field in a plane, then uses wavevector frequency-domain methods to project the field through layered media and to an arbitrary new plane, not necessarily parallel to the initial plane. The approach is valid for longitudinal propagation through liquid layers and in solids, such as soft tissues, that can be approximated as viscous liquids. The algorithm is verified by propagating the field from a 0.5 MHz planar transducer through a combination of rubber, plastic, and water layers. Hydrophone measurements indicate correlation between measured and simulated fields for angles below the longitudinal critical angles of the layered materials.**

I. Introduction

Planar projection methods use signal information in a single plane to provide the signal at any other point in space or time. Although a variety of algorithms have been described [1]–[8], the methods generally relate the field between two spatially or temporally separated planes by a projection operator in the wavevector-frequency domain or the wavevector-time domain. Stepanishen and Benjamin [2] first described the forward and backward projection technique in acoustics for propagating transient acoustic signals within a sourceless, homogeneous medium.

A major advantage of planar projection methods [2], as well as other wavevector and frequency domain methods [9], [10], is a substantial reduction in computation time as compared to integral finite element or finite-difference algorithms. As a result of their efficiency, the projection techniques have been applied to a wide number of problems, both linear and nonlinear [11], in which homogeneous medium may be assumed. Such uses include aberration correction [12], transducer characterization [13], full-field reconstruction [7], and the projection of transient and localized waveforms [14], [15].

The present study expands the wavevector-frequency domain projection method to include first-order propagation through randomly oriented, dissipative, layered media. Other notable studies have described the inclusion of layers [16], [17], absorption [18], and scattering [18] in planar projection methods, but they have been limited to cases of parallel layers. We describe, explicitly, a propagation algorithm derived from Stokes linear equation, which introduces several novel aspects to the wavevector-frequency domain planar projection. The projection operator is extended to include a passive rotation in wavevector space that allows the field to be projected along arbitrary axes not necessarily perpendicular to the measurement plane. Inclusion of this rotation allows signals to be efficiently projected toward a source that is located away from the measurement axis. The method also includes the effects of dispersion arising from the relaxation time of the media. And, the method is combined with ray theory to describe the propagation through randomly oriented layers.

To verify the algorithm, a series of layered cases are simulated and compared with experimental measurements performed at ultrasonic frequencies in a water tank. Correlation between the model and the experiment are found at incident angles less than the critical angle for fluid interfaces. These examples have direct application in layered biological media [19], in which the method may be used to propagate an ultrasound beam through sections of layered soft tissue or bone for diagnostic or therapeutic purposes.

Manuscript received June 10, 2002; accepted June 19, 2003. This work was supported by grants CA 46627 and CA 76550 from the National Institutes of Health.

The authors are with the Department of Radiology, Harvard Medical School, Brigham and Women's Hospital, Boston, MA 02115 (e-mail: gclement@hms.harvard.edu).

II. Theory

A. Planar Propagation

The projection problem assumes a generalized pressure field with an acoustic pressure $p(r,t)$ that satisfies the linearized Stokes equation [20]:

$$\left(1+\tau\frac{\partial}{\partial t}\right)\nabla^2 p(r,t)=\frac{1}{c^2}p(r,t), \tag{1}$$

where c is the real sound speed and τ is the relaxation time for the medium. Both of these quantities are, in general, functions of frequency. The projection is considered in Cartesian coordinates to relate the field between two planes at z_0 and z. A Helmholtz equation:

$$\left(\frac{\partial^2}{\partial z^2}+k^2\right)p(k_x,k_y,z,\omega)=0, \tag{2}$$

is obtained by the substitution of a Fourier integral with respect to the x and y coordinates into (1), where the Cartesian wavenumbers are given by k_x and k_y and ω is

the angular frequency. This equation is expressed in terms of a complex wavenumber k given by:

$$k = \sqrt{\frac{\omega^2}{c^2}\frac{1}{1+i\tau\omega} - k_x^2 - k_y^2}, \tag{3}$$

To propagate the field in a plane at a distance z_0 in front of a source to a new plane z, the advanced solution of (2) is used:

$$p(k,z) = p(k,z_0)e^{ik(z-z_0)}. \tag{4}$$

In the wavevector-frequency domain, the field over the plane z_0 is related to the field at any other plane z by a simple transfer function given in the right-hand side in (4). It is easily seen that, when the relaxation constant is set to zero, the amplitudes of any two parallel planes within the propagation band limit $\frac{\omega^2}{c^2} \geq k_x^2 + k_y^2$ are identical in amplitude and vary only in phase. When attenuation or layers are considered in the media, the transfer function must be modified [18], [21].

B. Dispersion

The complex wavenumber given by (3) is expressed in terms of the relaxation constant, τ, which is particular to a given layer type and is generally not known. However, (3) may be separated into its real and imaginary parts such that:

$$\kappa + i\alpha = \frac{\omega}{c}\frac{1}{\sqrt{1+i\tau\omega}}. \tag{5}$$

The imaginary part of the wavenumber is the absorption coefficient, which is assumed known. In terms of the relaxation constant:

$$\begin{aligned}\kappa &= \frac{\omega}{c}\frac{1}{\sqrt{2}}\left[\frac{\sqrt{1+(\omega\tau)^2}+1}{1+(\omega\tau)^2}\right]^{\frac{1}{2}} \\ \alpha &= -\frac{\omega}{c}\frac{1}{\sqrt{2}}\left[\frac{\sqrt{1+(\omega\tau)^2}-1}{1+(\omega\tau)^2}\right]^{\frac{1}{2}},\end{aligned} \tag{6}$$

which provides a pair of coupled equations, allowing κ to be determined if the frequency-dependent absorption coefficient of a given layer is known (empirically or otherwise). Substitution of (5) into (4), and separation of the real and imaginary exponents using DeMoivere's formula [22] results in a new projection function:

$$p(k_x,k_y,\omega,z) = p(k_x,k_y,\omega,z_0)e^{(z-z_0)R^{1/2}\sin\frac{\xi}{2}}e^{i(z-z_0)R^{1/2}\cos\frac{\xi}{2}}, \tag{7}$$

where,

$$R = \sqrt{(\alpha^2+\kappa^2-k_x^2-k_y^2)^2 + 4\alpha^2\kappa^2} \tag{8}$$

and

$$\xi = \tan^{-1}\left[\frac{2\kappa\alpha}{\kappa^2+\alpha^2-k_x^2-k_y^2}\right], \tag{9}$$

noting that κ and α are coupled by (6). The first exponential term in (7) represents the decay in amplitude experienced as a function of k_x and k_y. Similarly, the second exponential term provides the phase shift.

C. Rotation

The spatial Fourier transform projection method is often referred to as the angular spectrum approach because the transform may be viewed as an angular decomposition of the field. That is, each point $p(k_x,k_y,\omega,z_0)$ describes a planar wave with a wavenumber $\sqrt{k_x^2+k_z^2}$ passing through the measurement plane at an angle equal to $\psi_x = \sin^{-1}k_x\frac{c}{\omega}$ from the z-axis in the x-z plane and with a wavenumber $\sqrt{k_y^2+k_x^2}$ at an angle $\psi_y = \sin^{-1}k_y\frac{c}{\omega}$ in the y-z plane. The amplitude of the wave is equal to the modulus of p. This concept is illustrated for a two-dimensional case in Fig. 1. The figure may also be viewed at a two-dimensional projection of the three-dimensional case in which the polar angle θ and azimuthal angle ϕ are given by:

$$\begin{aligned}\tan\psi_x &= \tan\theta\cos\phi \\ \tan\psi_y &= \tan\theta\sin\phi\end{aligned}. \tag{10}$$

For a transient signal, each temporal frequency component possesses a unique angular spectrum, so that a generalized waveform will constitute a three-dimensional space (k_x,k_y,ω), consisting of two spatial frequency dimensions and one temporal frequency.

Viewing the field over the plane at z_0 as an angular decomposition, it becomes straightforward to perform a passive coordinate rotation. To orient the plane along a new projection axis, z_o', each point p in wavevector space is mapped to the rotated plane such that:

$$\begin{pmatrix}k_x'\\k_y'\\k_z'\end{pmatrix} = \hat{A}\left(\phi^{ROT},\theta^{ROT},\psi^{ROT}\right)\begin{pmatrix}k_x\\k_y\\k_z\end{pmatrix}, \tag{11}$$

where $\hat{A}\left(\phi^{ROT},\theta^{ROT},\psi^{ROT}\right)$ represents an Euler rotation matrix, ϕ^{ROT} is the azimuth of a vector along z_0' in the unrotated coordinate system, θ^{ROT} is the angle between z and z_0', and ψ^{ROT} is the third Eulerian angle that rotates about the z_0' axis. Projection along the new axis to an arbitrary new plane z' can be achieved using (4). The inverse Fourier transform performed after this mapping provides the pressure field in the plane rotated to $\left(\theta^{ROT},\phi^{ROT}\right)$. An interesting application of the rotation arises when the exact orientation of the source is not known. In this situation the source location can be obtained from the Fourier transform of the pressure field, taking the angles associated with maximum amplitude of $p(k_x,k_y,\omega,z_0)$.

D. Propagation Through Layers

Propagation through layered media in wavevector space is achieved by determining how the layers distort each point in the space. An arbitrary field incident upon a series

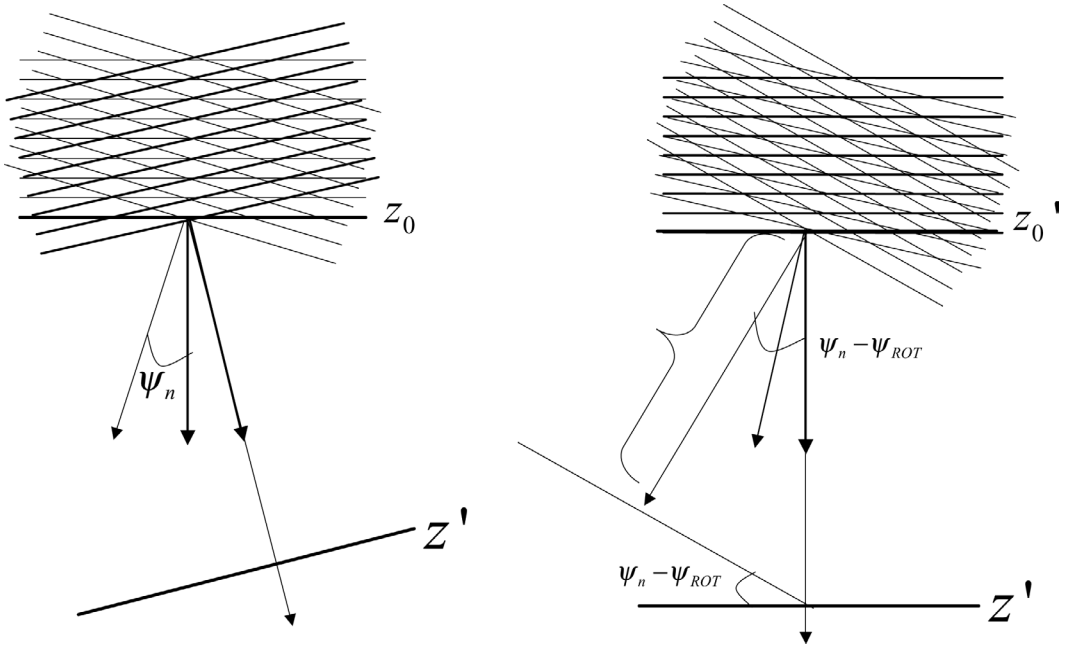

Fig. 1. Two-dimensional illustration of the spectral decomposition (left) and rotation (right). The field initially at the plane perpendicular to z_0 is rotated and projected to a new plane perpendicular to z'.

of planar layers is first considered, as this will be the basis for later describing propagation through curved surfaces. Each wavevector component over the plane at z_0 is associated with a wavevector $k_{0xy}(\omega) = k_x(\omega)\hat{i} + k_y(\omega)\hat{j}$, where the indices (x, y) indicate the position of the component in k-space. The angle of incidence between a given wavevector and the vector normal to the outer surface of the nth layer is given by $\gamma_{i_{nxy}}(\omega)$, and the transmitted angle by $\gamma_{t_{nxy}}(\omega)$. For a layer with sound speeds c_n and density ρ_n, the pressure transmission coefficient at its lower interface is given by [23]:

$$T_{nxy}(\omega) = \frac{2\rho_{n+1}c_{n+1}\cos\gamma_{i_{nxy}}\cos\gamma_{t_{nxy}}}{\rho_n c_n \cos\gamma_{t_{nxy}} + \rho_{n+1}c_{n+1}\cos\gamma_{i_{nxy}}}, \tag{12}$$

where the incident and transmitted angles are understood to be a function of frequency. Because the problem has been decomposed into a series of plane waves, transmission of the field from the outer surface to the next layer may be treated either by using a ray method or by applying the continuity of the pressure and normal particle velocity at the interface. The ray method is described below in detail, as it leads to the general case of propagation through nonparallel layers. In this first-order propagation, multiple reflections within the layers are neglected, although such higher order reflections could readily be added as necessary.

Regardless of whether or not the layers are parallel, the transfer function readily may be written in a closed form. In addition to the thickness across the z-axis, z_n, the sound speed c_n, and density of each layer ρ_n, it is necessary that the unit vectors normal to the layer surfaces $\hat{n}_n$ be calculated. For a given initial wavevector k_{0xy}, the ray path from $(0, 0, z_0)$ between any two surface interfaces traverses

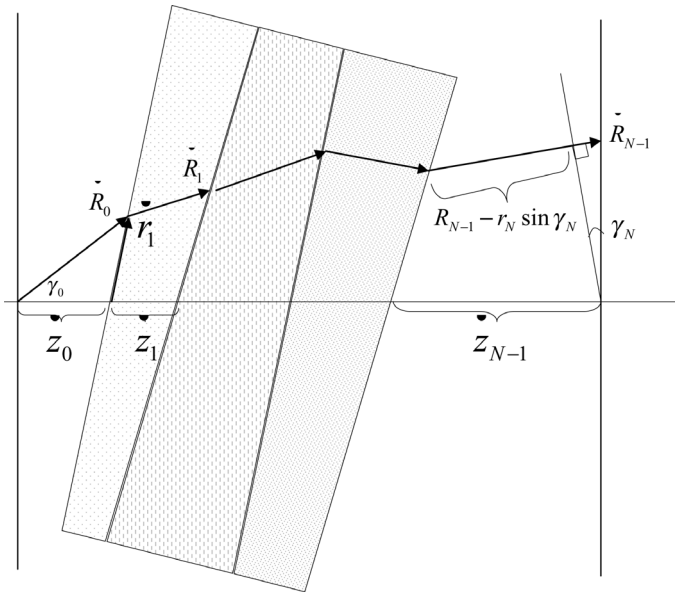

Fig. 2. The field is decomposed into planar waves, which are directed through layers, keeping track of the overall phase variation, amplitude, and orientation.

a distance of:

$$|R_{nxy}| = \frac{(z_{nxy} - r_{nxy}) \cdot \hat{n}_{n+1}}{\hat{k}_{nxy} \cdot \hat{n}_{n+1}}, \tag{13}$$

where, as depicted in Fig. 2, r_{nxy} is the vector extending along the layer from the z-axis to the intercept of the layer with the ray. The unit vector along the wavevector's path is given by $\hat{k}_{nxy}$. Again, the frequency dependence on the wavevector orientation is understood. It follows that the ray position vector must be equal to

$R_{nxy} = |R_{nxy}|\,\hat{k}_{nxy}$. Although the initial wavevector orientation, $\hat{k}_{0xy}$, is known, the direction of the wavevector in the first and subsequent layers must be calculated using the relation [24]:

$$\frac{1}{c_n}\left(\hat{n}_{n+1}\times\hat{k}_{nxy}\right)=\frac{1}{c_{n+1}}\left(\hat{n}_{n+1}\times\hat{k}_{n+1xy}\right), \tag{14}$$

which is a consequence of Snell's law in three-dimensional space that requires the incident wavevector, the transmitted wavevector, and the normal vector all be in the same plane. The transmitted wavevector on the right-hand side of (14) may be obtained by crossing both sides of the equation with $\hat{n}_{n+1}$. Using cross-product relations, it may be shown that:

$$\hat{k}_{n+1xy}=\frac{c_{n+1}}{c_n}\left(\hat{k}_{nxy}-\cos\gamma_{i_{n+1xy}}\hat{n}_{n+1}\right)+\cos\gamma_{i_{n+1xy}}\hat{n}_{n+1}. \tag{15}$$

The incident unit wavevector of the nth layer is simply equal to the transmitted wave of the $(n-1)$st layer. With the exception of the 0th layer shown in Fig. 2 it also is necessary to find r_{nxy} in order to calculate (13). Given the thickness across the z-axis of each layer, the point of intersection of ray R_n with the surface of the $n+1$ layer is:

$$r_{n+1}=R_n+r_n-z_n. \tag{16}$$

Over a series of N layers, the phase of a ray reaching the Nth plane $\phi_R\left(k_{Nxy},\omega\right)$ is the sum of the phase contributions over each path length given by (13). The spatial phase at the plane z, is related to the ray phase at N by: $\phi_N\left(k_{Nxy},\omega\right)=\phi_R\left(k_{Nxy},\omega\right)-2\pi k_N r_N\sin\gamma_{Nxy}$, as illustrated in Fig. 2. A ray leaving the initial plane with a polar angle $\gamma_{0xy}(\omega)$ will arrive at the plane z with a new orientation $\gamma_{Nxy}(\omega)$ determined by the $N-1$ unit vector $\hat{k}_{N-1}$.

$$\phi\left(k_{Nxy},\omega,z\right)=\phi\left(k_{0xy},\omega,z_0\right)+\sum_{n=0}^{N-1}k_n\frac{\left(z_n-r_n\right)\cdot\hat{n}_{n+1}}{\hat{k}_n\cdot\hat{n}_{n+1}}-\sin\gamma_{Nxy}(\omega), \tag{17}$$

given $\phi\left(k_{0xy},\omega,z_0\right)$, the phase of $p\left(k_x,k_y,\omega,z_0\right)$ at the initial plane.

The pressure over the plane at z can be expressed in terms of the ray phase presented in (17) and the transmission coefficient in (12) by:

$$p\left(k_{Nxy},\omega,z\right)=p\left(k_{0xy},\omega,z_0\right)e^{-i\sin\gamma_{Nxy}(\omega)}\left[\sum_{n=1}^{N-1}T_{nxy}(\omega)e^{i\phi_N\left(k_{Nxy},\omega,z\right)}\right], \tag{18}$$

where the terms in square brackets on the left-hand side of (18) can be viewed as an operator that maps the field from k_0-space to a new k_N-space. In practice, this mapping requires interpolation to produce a linearly spaced matrix at z.

E. Nonplanar Surfaces

The layered-projection method may be used for the propagation of a field through a curved surface, provided the surface is sufficiently smooth relative to the highest relevant wavenumber. The field is projected to a plane near the surface and is then divided into a series of virtual sources. The region of the surface penetrated by a given source is approximated as planar, so the actual surface over the beamwidth of the source must agree with this approximation to at least within ¼ λ (or less, depending upon the desired tolerance) of the maximum frequency $k_{\max}$. At the same time, the source diameter S must be large enough that the smaller frequency components of the source are in the near field relative to the Rayleigh distance, requiring $S>\sqrt{z/2k_{\min}}$, where $k_{\min}$ is the smallest appreciable frequency of the signal and z is the distance from the starting plane to the surface. The projection may be performed if these requirements can be met. It is noted that, although the planar field is uniquely divided into a continuous series of sources, the fields of the sources will overlap on the surface.

When propagating through multiple layers, each of the surfaces is segmented as described above. It is possible that components with high-transmission angles will leave the surface of interest. Although the algorithm may be used to treat such occurrences, the discussion is beyond the scope of the current topic. Hence, the wavevector components are assumed to remain within the segmented regions illustrated in Fig. 2.

III. Simulation

Several propagation examples were considered in order to demonstrate the projection method and verify it with laboratory measurements. The examples considered harmonic signals propagated through layered geometries that could be actualized readily in experiments. These relatively simple situations are relevant to more complex spatial and temporal problems because the algorithm decomposes all broadband and nonplaner problems into these simple cases. The examples also helped to identify the model's limitations and to provide directions for future work.

Specifically, propagation was simulated through three parallel layers, five parallel layers, and three nonparallel layers. The dimensions, orientations, sound speeds, and densities of the layers corresponded to plastic and rubber materials used in experiments to verify the simulations. Diagrams of the layers are given in Fig. 3. The source for the simulations was an 18-mm diameter circular piston, which was operated at frequencies ranging from 0.4 MHz to 0.7 MHz. In the three-layer simulation, a water-plastic-water interface was considered ($\rho_w=1000$ kg/m^3, $c_w=1.498$ m/s, $\rho_p=1187$ m/s, $c_p=2185$ m/s). The plastic layer (Plastic 1) was 11.8 mm thick, the distance from the source to the measured plane was 121 mm and the distance

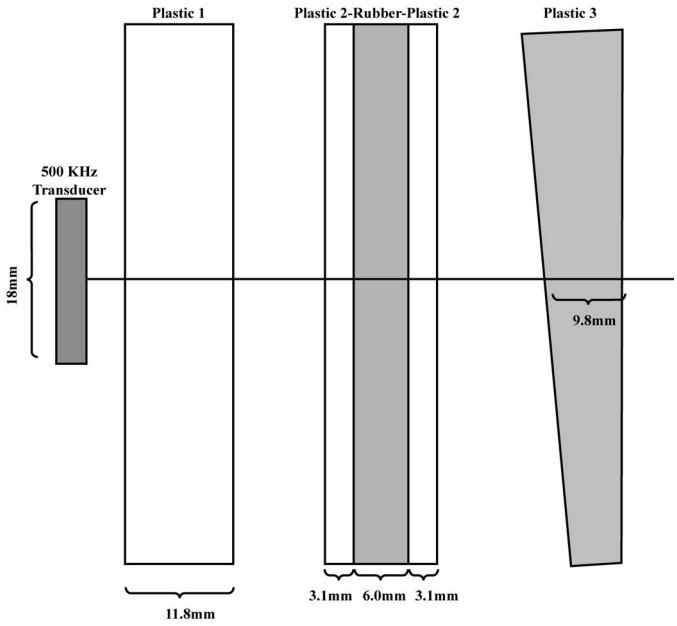

Fig. 3. Illustration of the transducer diameter and the thickness of the materials used to verify the projection algorithm.

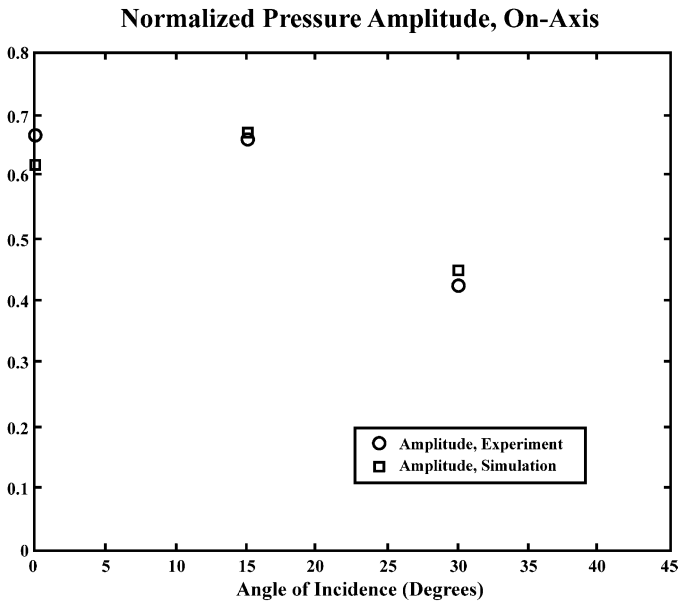

Fig. 4. Measured (circles) and calculated (squares) on-axis normalized pressure amplitude as a function of incident angle through a planar plastic plate.

TABLE I
SUMMARY OF MATERIAL PROPERTIES.

Material	Thickness (mm)	ρ (kg/m^3)	c (m/s)
Water	Variable	1000	1498
Plastic 1	11.8	1187	2185
Plastic 2	3.1	1236	2770
Rubber	6	1089	1520
Plastic 3	9.8*	1233	2485

* radius across transducer axis with surface normal to the transducer face.

from the plastic inner surface to the source was 61 mm. The second parallel-plate simulation was calculated for a field through five layers consisting of water-plastic rubber-plastic-water ($\rho_r = 1089\,\mathrm{kg/m^3}$, $c_r = 1520\,\mathrm{m/s}$). The plastic layers (Plastic 2) were each 3.1 mm thick, and the rubber layer was 6.0 mm thick. The distance from the source to the measured plane was 49 mm, and the distance from the plastic inner surface to the source was 60 mm. The third simulation involved a water-plastic-(Plastic 3)-water wedge ($\rho_w = 1233\,\mathrm{kg/m^3}$, $c_w = 2485\,\mathrm{m/s}$). The wedge surfaces differed by an angle of 7.05°. The material properties and dimensions are summarized in Table I.

A numeric algorithm was implemented in Matlab, using matrix-based operations to calculate (18) for parallel layers and for nonparallel layers. The pressure field representation in the wavevector-domain $p\,(k_{0xy}, \omega, z_0)$ was achieved using discrete approximation to the Fourier integral using the matrix operation:

$$p_{k_x k_y \omega} = \frac{1}{2\pi}\left(\begin{bmatrix} p_{x_1 y_1} & p_{x_1 y_n} \\ p_{x_n y_1} & p_{x_n y_n} \end{bmatrix}_{\omega} \begin{bmatrix} e^{ik_{y_1} y_1} & e^{ik_{x_n} x_1} \\ e^{ik_{y_1} y_n} & e^{ik_{x_n} x_n} \end{bmatrix}\right)^T \begin{bmatrix} e^{ik_{x_1} x_1} & e^{ik_{y_n} y_1} \\ e^{ik_{x_1} x_n} & e^{ik_{y_n} y_n} \end{bmatrix} \Delta k_x \Delta k_y \quad (19)$$

for each frequency (a single temporal frequency was used in the present continuous wave (CW) examples) with a spatial frequency resolution of $\Delta k_x = \Delta k_y = 2.1 \times 10^{-4}$ rad/m. Operations were performed on a 1-GHz AMD-Based PC (AMD, Sunnyvale, CA). A typical projection of a complex 128×128 matrix through five layers took approximately 30 seconds to calculate. A projection of the same matrix through five nonparallel layers took less than 1 minute.

IV. Experimental Procedure

Propagation experiments were set up in a water tank to verify the numeric results described above. Plastic and rubber plates were pressed together into layers corresponding to the three layer (water-Plastic 1-water), and five layer (water-Plastic 2-rubber-Plastic 2-water) simulations. Measurements were performed in degassed and deionized water in a tank padded with rubber to inhibit reflections from its walls. Ultrasound signals were generated by a 3-cm diameter piezo-composite ultrasound transducer and received with a 0.2 mm Polyvinylidene difluoride (PVDF) hydrophone (Precision Acoustics, Dorchester, UK). Prior to hydrophone measurement, one of the layered plates was placed between the hydrophone and transducer at an angle that was controlled by a rotational stepping motor (Parker, Irwin, PA). A three-dimensional linear positioning system (Velmex, Bloomfield, NY, Model VP9000) allowed the hydrophone to be scanned over a measurement area centered about the transducer's axis of symmetry. Transducer signals were generated by an arbitrary waveform generator (Wavetek, Norwich, UK, Model 305) fed to a power amplifier (ENI, Rochester, NY, Model 2100L).

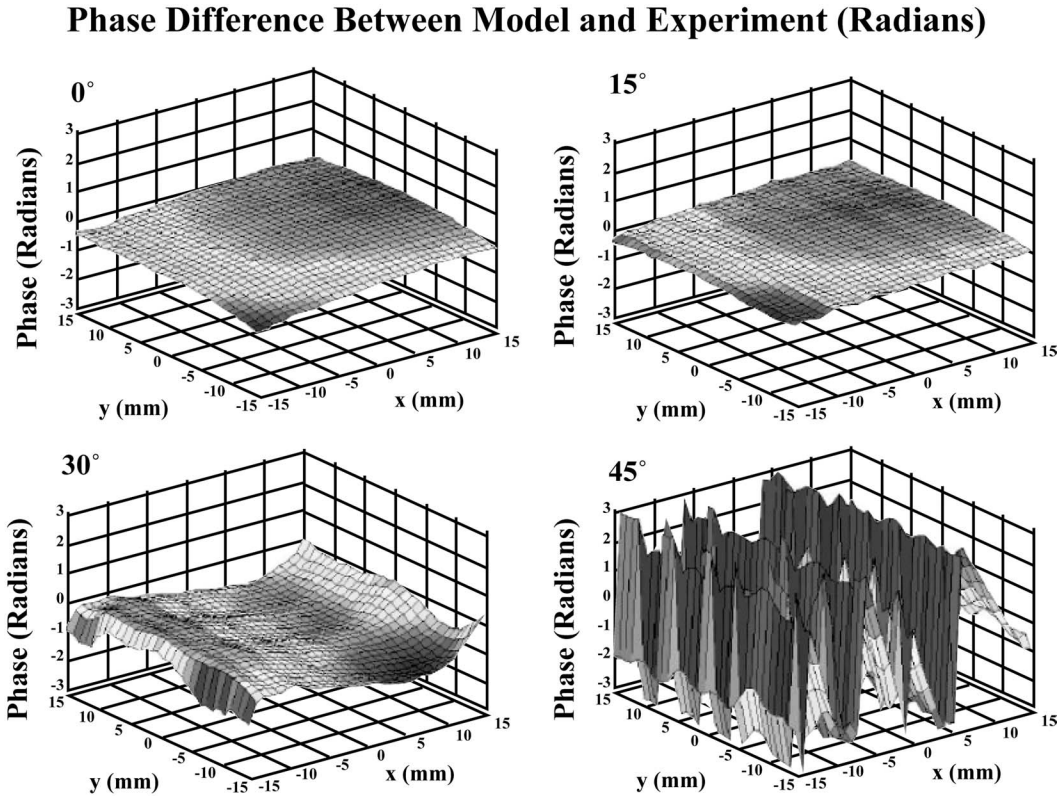

Fig. 5. Subtraction of the measured and calculated phases through a plastic plate over a 30 mm by 30 mm measurement plane at 0°, 15°, 30°, and 45°.

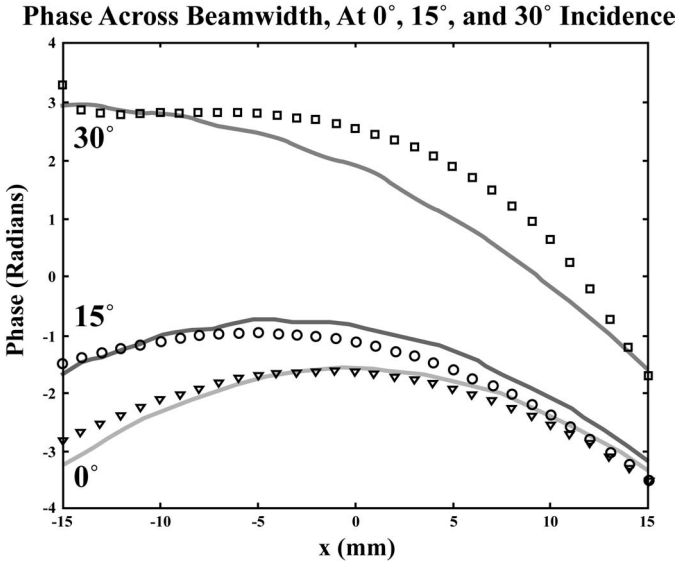

Fig. 6. Measured and calculated (solid line) phases in a line over the beamwidth, at 0° (triangles), 15° (circles), and 30° (squares).

The hydrophone's voltage response was sent though a Precision Acoustics pre-amp and an amplifier (Preamble Instruments, Beaverton, OR, Model 1820) before it was recorded by a digital oscilloscope (Textronix, Wilsonville, OR, Model 380). Both the scan position and the data acquisition were computer controlled.

V. Results

A. Propagation Through Parallel Layers

The 11.8-mm thick acrylic plate was placed in the test tank, and the acoustic transmission was measured on the transducer's axis of symmetry 121 mm from its face. The measurement was repeated for incident angles of 0°, 15°, 30°, and 45° at 500 kHz. Agreement between the measured and simulated waveforms was evaluated by comparing the overall amplitude shape, as well as amplitude and phase magnitudes over the 30 mm by 30 mm measurement plane. Numeric and laboratory measurements both were calculated as a fraction of the peak value measured in water with no plate present, allowing a relative comparison of the simulated and experimental fields. Correlation was observed between the measured and predicted fields at incident angles below 31°, which is the longitudinal critical angle for the signal's spectral peak. The on-axis error between the measured and simulated pressure amplitude was calculated as the difference between the modulus of the measured and simulated pressure fields divided by the measured result. The discrepancy was found to be 9.1% at 0° incidence, 0.05% at 15° incidence, 5.1% at 30° incidence, and 98% at 45°. The mean error of all points in the 30 mm by 30 mm measurement plane 19% at 0° incidence, 6% at 15° incidence, 79% at 30° incidence, and 96% at 45° incidence. The simulated and measured on-axis

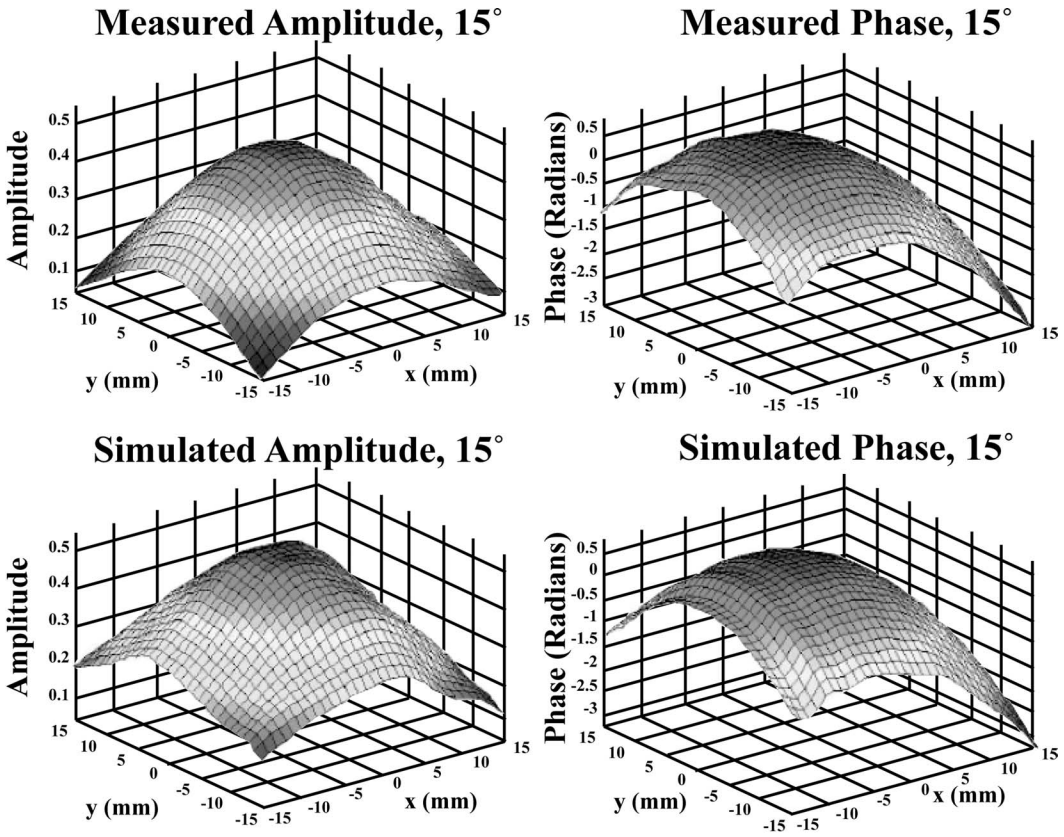

Fig. 7. Measured (top) and simulated (bottom) amplitudes and phase through a five-layer, water-plastic-rubber-plastic-water field 15°.

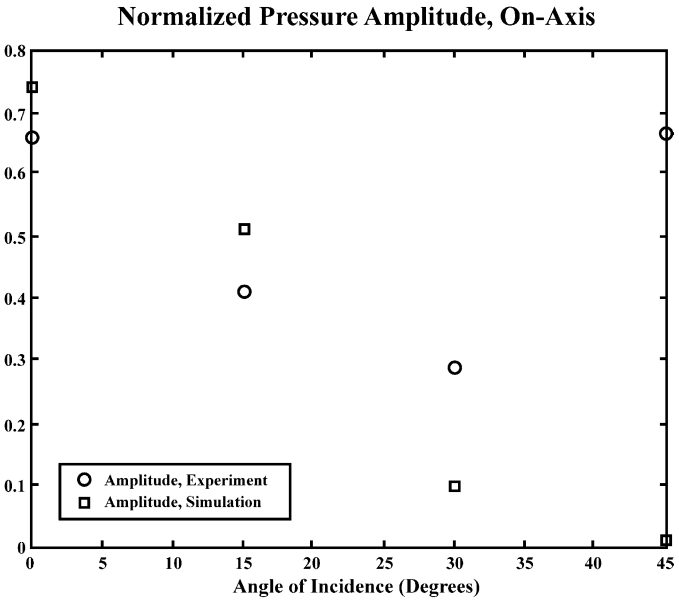

Fig. 8. Measured (circles) and calculated (squares) on-axis normalized pressure amplitude as a function of incident angle through a five-layer, water-plastic-rubber-plastic-water field.

pressure amplitudes below the critical angle are presented in Fig. 4.

The mean phase difference between all measured and simulated points, shown in Fig. 5, was calculated by summing the phase errors at each point over the 30 cm by 30 cm measurement plane at 1-mm intervals. The mean phase difference was found to be 5.3° ± 13° at 0° incidence, 7.0° ± 9.8° at 15° incidence, and 30° ± 23° at 30° incidence. The uncertainty ranges are over two standard deviations of the data. The numeric and measured phases for the angles below the critical angle are presented in Fig. 6 for radial lines crossing the center of the measurement plane. Again, beyond the critical angle, the measured signal is primarily due to lateral modes of vibration in the plastic, which are neglected in the present model. The large uncertainty between the measured and modeled data (−3.9° ± 99° at 45° incidence) demonstrates this lack of correspondence.

Similar analysis was performed for measurements of the 6.0-mm rubber plate sandwiched between two 3.1-mm plastic plates. Fig. 7 shows the measured and simulated amplitude and phase after passing through the plate at an incident angle of 15°. Fig. 7 illustrates the shifting of the layers (in this case the amplitude is shifted to the right and the phase is shifted to the left), and the simulation's ability to track these shifts. The on-axis error between the measured and simulated pressure amplitude was 12% at 0° incidence, 25% at 15° incidence, 68% at 30° incidence, and 99% at 45° incidence. The simulated and measured on-axis pressure amplitudes are presented in Fig. 8. The mean error of all points in the 30 mm by 30 mm measurement plane 17% at 0° incidence, 17% at 15° incidence, 57% at 30° incidence, and 98% at 45° incidence. The mean phase difference between all measured and simulated points was

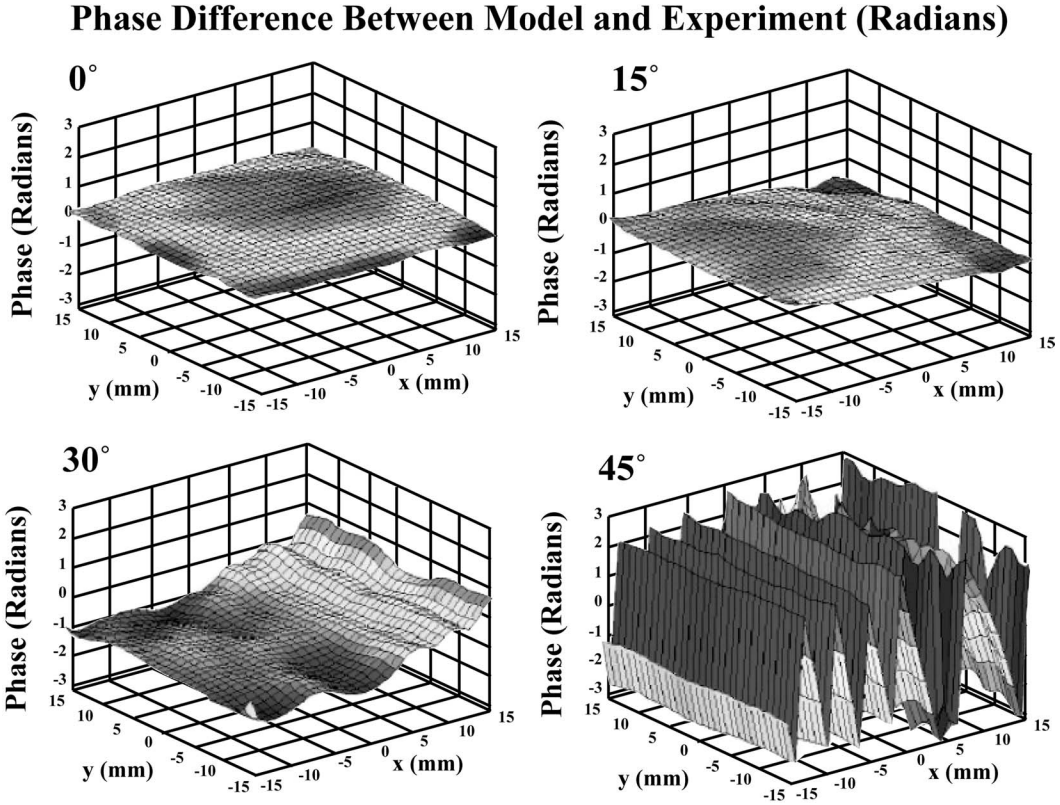

Fig. 9. Subtraction of the measured and calculated phases through a five-layer, water-plastic-rubber-plastic-water field over a 30 mm by 30 mm measurement plane in water at 0°, 15°, 30°, and 45°.

found to be 13° ± 6.9° at 0° incidence, −8.7° ± 12° at 15° incidence, and −39° ± 26° at 30° incidence. These differences are illustrated in Fig. 9.

B. Propagation Through Nonparallel Layers

The polystyrene-polyester based wedge in Fig. 4 was oriented at various angles between the transducer's propagation axis and the wedge surface. Field measurements were performed at orientation angles equal to −22°, −15°, 0°, 15°, and 22°, in which the angle refers to the difference angle between the transducer face and the wedge surface closest to the hydrophone. Negative angles correspond to the direction producing a longer axial length [z_2 in (16)] through the wedge. The on-axis error between the measured and simulated pressure amplitude was observed to be systematically higher for the simulation, as illustrated in Fig. 10, with errors ranging from 5.8% at 15°, to 32.1% at −22°. The mean error over all points in the measured plane ranged from 8% at 0° incidence to 19% at 22° incidence.

With the exception of the propagation at an incident angle of 22°, the simulated ultrasound phase successfully predicted the ultrasound phase to within 20° of the measured values. The mean phase difference of all measured points, shown in Fig. 11, was found to be 18° ± 12° at −22° incidence, 15° ± 9.5° at −15° incidence, 19° ± 8.7° at 0° incidence, 8.9° ± 8.8° at 15° incidence and 67° ± 14° at 22° incidence.

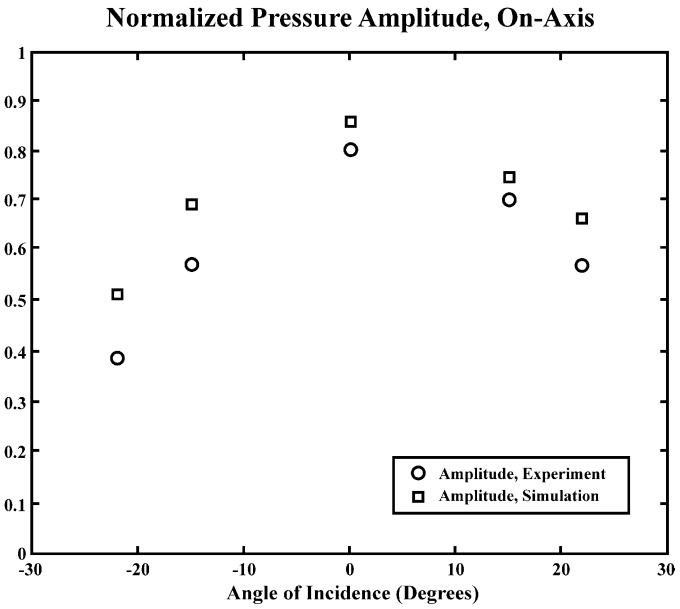

Fig. 10. Measured (circles) and calculated (squares) on-axis normalized pressure amplitude as a function of incident angle through a planar plastic plate.

VI. Discussion

The layered-projection model applies the forward and backward planar projection method to the complex problem of propagating through inhomogeneous materials. This computationally efficient and adaptable method is

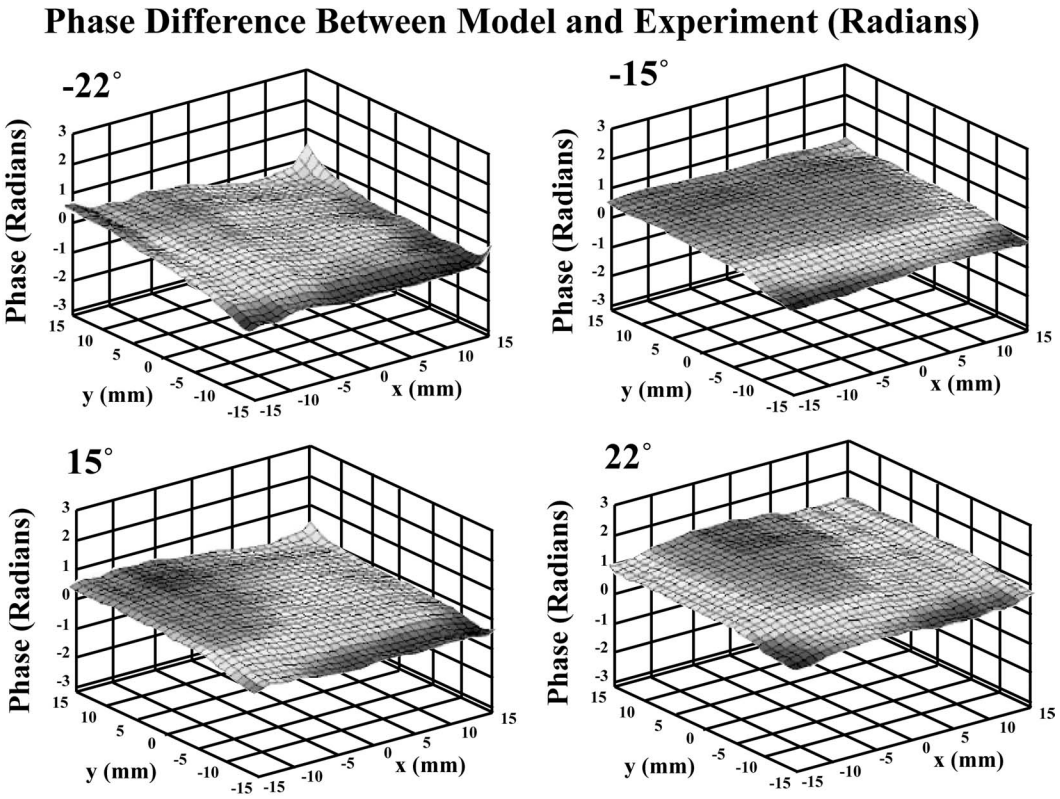

Fig. 11. Subtraction of the measured and calculated phases through a plastic wedge over a 30 mm by 30 mm measurement plane at −22°, −15°, 15°, and 22°.

used with a ray-based theory to propagate an arbitrary waveform through any number of arbitrarily oriented layers.

In its present form, the algorithm considers only longitudinal propagation in fluid-like materials. Hence, the effects of mode coupling in solids are neglected, which will cause the model to break down at high incident angles. This is evident in the example of the 11.8-mm plastic plate, in which the amplitude and phase of the transmitted signal is poorly predicted beyond the critical angle for longitudinal propagation.

The model requires that the structure of the medium be known a priori and is practical only for applications in which this is feasible. In biological and medical applications, this information could be obtained from X-ray computed tomography (CT) or magnetic resonance imaging (MRI). Potential uses of the method include aberration correction for ultrasound imaging as well as for therapy. For any physical applications, the effects of imperfections on the source array can be included easily by using planar measurements of the transducer's pressure field as the starting plane for the algorithm.

Phase and amplitude aberration correction could be performed by segmenting the propagation medium as described in Section II, and propagating through layers within the section. The acoustic pressure then can be calculated by summing the contributions of the different segments. To restore a destroyed or distorted focus, the segmented data could be used to determine the magnitude of phase and amplitude distortion experienced through each segment, then offset by adjusting the individual elements in a transducer array. In this manner, the goal is to combine the fields so that the individual segments arrive in phase at the focal point. A previous study [25] through skull bone predicts that, even if a significant number of array elements contain a high-phase error, improvement in a focus through skull bone is possible. Specifically it was indicated that if 50% of all element contributions by a 1000 point array deviated by more than 38°, it was still possible to improve the focal peak to 76% of the value expected with perfect phasing.

We already have applied a special case of the projection approach toward a study on transskull focusing, which was performed in parallel with the present theoretical study [26]. In this focusing experiment, human skulls were approximated as a single-layer structure. The approach segmented the skulls into 320 single-layer plates, which were evaluated using a special case of the propagation theory, valid only for parallel layers. The method successfully restored an ultrasound focus through 10 ex vivo skulls, using a hemisphere-shaped array, which generally kept the ultrasound angles incident with the skull under 20°. Future transskull work will concentrate on using a more precise version of the model in which the skull is modeled as a three-layer, nonparallel structure.

The examples included in this paper illustrate how the theory may be used and indicate some of its limits. The method was able to model the propagation of a planar

transducer through layers when the incident angle was small enough for shear modes to be neglected. The algorithm was particularly successful at ultrasound phase estimation in which correlation was observed even near the longitudinal critical angles. Sources of experimental error are expected to arise from error in the sound-speed estimates, density, and attenuation, as well as measurements of material thickness, angle, and orientation angle. Also, contributions by higher order reflections, which are neglected in the present work, are a possible source of error in the numeric calculation.

This preliminary study demonstrates the ability of a wavevector planar projection model to predict the behavior of waveforms propagated through layered media, given a priori knowledge of the propagation media. The algorithm was effective in predicting the distortion caused by phantom-layer models at incident angles below Snell's critical angle. Based on the results of this approach, we surmise that the algorithm may be used for a wide range of noninvasive focusing and aberration correction uses in which longitudinal modes are dominant, such as focusing through biological tissue layers.

References

[1] E. G. Williams and J. D. Maynard, "Holographic imaging without the wavelength resolution limit," *Phys. Rev. Lett.*, vol. 45, no. 7, pp. 554–557, 1980.

[2] P. R. Stepanishen and K. C. Benjamin, "Forward and backward projection of acoustic fields using FFT methods," *J. Acoust. Soc. Amer.*, vol. 71, pp. 803–812, 1982.

[3] R. Reibold and F. Holzer, "Complete mapping of ultrasonic fields without the wavelength limit," *Acustica*, vol. 58, pp. 11–16, 1985.

[4] M. E. Schafer and P. A. Lewin, "Transducer characterization using the angular spectrum approach," *J. Acoust. Soc. Amer.*, vol. 85, pp. 2202–2214, 1989.

[5] M. Forbes, S. V. Letcher, and P. R. Stepanishen, "A wave vector, time-domain method of forward projecting time-dependent pressure fields," *J. Acoust. Soc. Amer.*, vol. 90, pp. 2782–2793, 1991.

[6] P. T. Christopher and K. J. Parker, "New approaches to the linear propagation of acoustic fields," *J. Acoust. Soc. Amer.*, vol. 90, pp. 507–521, 1991.

[7] D.-L. D. Liu and R. C. Waag, "Propagation and backpropagation for ultrasonic wavefront design," *IEEE Trans. Ultrason., Ferroelect., Freq. Contr.*, vol. 44, pp. 1–13, 1997.

[8] P. Wu and T. Stepinski, "Extension of the angular spectrum approach to curved radiators," *J. Acoust. Soc. Amer.*, vol. 5, pp. 2618–2627, 1999.

[9] N. N. Bojarski, "The k-space formulation of the scattering problem in the time domain," *J. Acoust. Soc. Amer.*, vol. 72, pp. 570–584, 1982.

[10] T. D. Mast, L. P. Souriau, D.-L. D. Liu, M. Tabei, A. I. Nachman, and R. C. Waag, "A k-space method for large-scale models of wave propagation in tissue," *IEEE Trans. Ultrason., Ferroelect., Freq. Contr.*, vol. 48, pp. 341–354, 2001.

[11] C. J. Vecchio and P. A. Lewin, "Finite amplitude acoustic propagation modeling using the extended angular spectrum method," *J. Acoust. Soc. Amer.*, vol. 95, pp. 2399–2408, 1994.

[12] G. T. Clement and K. Hynynen, "Field characterization of therapeutic ultrasound phased arrays through forward and backward planar projection," *J. Acoust. Soc. Amer.*, vol. 108, pp. 441–446, 2000.

[13] D.-L. Liu and R. C. Waag, "Correction of ultrasonic wavefront distortion using backpropagation and a reference waveform method for time-shift compensation," *J. Acoust. Soc. Amer.*, vol. 96, pp. 649–660, 1994.

[14] G. T. Clement, R. Liu, S. V. Letcher, and P. R. Stepanishen, "Forward projection of transient signals obtained from a fiber-optic pressure sensor," *J. Acoust. Soc. Amer.*, vol. 104, pp. 1266–1273, 1998.

[15] G. T. Clement, R. Liu, S. V. Letcher, and P. R. Stepanishen, "Temporal backward planar projection of acoustic transients," *J. Acoust. Soc. Amer.*, vol. 103, pp. 1723–1726, 1998.

[16] C. J. Vecchio, M. E. Schafer, and P. A. Lewin, "Prediction of ultrasonic field propagation through layered media using the extended angular spectrum method," *Ultrasound Med. Biol.*, vol. 20, pp. 611–622, 1994.

[17] Z. D. Qin, A. Tauriainen, J. Ylitalo, E. Alasaarela, and W. Lu, "Frequency domain compensation for inhomogeneous layers in ultrasound holography," *IEEE Trans. Ultrason., Ferroelect., Freq. Contr.*, vol. 36, pp. 73–79, 1989.

[18] M. E. Schafer, P. A. Lewin, and J. M. Reid, "Propagation through inhomogeneous media using the angular spectrum method," in *Proc. IEEE Ultrason. Symp.*, 1987, pp. 943–946.

[19] E. Kuhnickle, "Simulation calculations for monofrequent sound fields in layered media," in *Acoustical Imaging*. J. P. Jones, Ed. New York: Plenum, 1995, pp. 47–53.

[20] A. D. Pierce, *Acoustics, An Introduction to Its Physical Principles and Applications*. Woodbury, NY: Acoustical Society of America, 1989.

[21] M. E. Schafer, "Transducer characterization in inhomogeneous media using the angular spectrum method," Ph.D. dissertation, Dept. of Biomedical Engineering, Drexel University, Philadelphia, PA, 1988.

[22] E. B. Saff and A. D. Snider, *Fundamentals of Complex Analysis*. Englewood Cliffs, NJ: Prentice-Hall, 1976.

[23] L. E. Kinsler and A. R. Frey, *Fundamentals of Acoustics*. New York: Wiley, 1982.

[24] J. E. Marsden and A. J. Tromba, *Vector Calculus*. New York: Freeman, 1988.

[25] G. T. Clement and K. Hynynen, "Correlation of ultrasound phase with physical skull properties," *Ultrasound Med. Biol.*, vol. 28, pp. 617–624, 2002.

[26] G. T. Clement and K. Hynynen, "A noninvasive method for focusing ultrasound through the human skull," *Phys. Med. Biol.*, vol. 47, pp. 1219–1236, 2002.